Energy transfer mediated by asymmetric hydrogen-bonded interfaces

Published in final edited form as:
Chem Sci. 2012 February 1; 3(2): . doi:10.1039/C1SC00596K.

Energy transfer mediated by asymmetric hydrogen-bonded interfaces†

Elizabeth R. Young[a], **Joel Rosenthal**[b], and **Daniel G. Nocera**[c]

[a]Department of Chemistry, Amherst College, P.O. Box 5000, Amherst, MA, 01002-5000, USA

[b]Department of Chemistry and Biochemistry, University of Delaware, Newark, DE, 19716, USA

[c]Department of Chemistry, Massachusetts Institute of Technology, 77 Massachusetts Avenue, Cambridge, MA, 02139-4307, USA. nocera@mit.edu; Tel: +1 617 253 5537

Abstract

Amidine-appended ferrocene derivatives form a supramolecular assembly with Ru(II)(bpy-COOH)$(L)_2^{2+}$ complexes (bpy-COOH is 4-CO_2H-4′-CH_3-bpy and L = bpy, 2,2′-bipyridine or btfmbpy, 4,4′-*bis* (trifluoromethyl)-2,2′-bipyridine). Steady-state, time-resolved spectroscopy and kinetic isotope effects establish that the metal-to-ligand charge transfer excited states of the Ru(II) complexes are quenched by proton-coupled energy transfer (PCEnT). These results show that proton motion can be effective in mediating not only electron transfer (ET) but energy transfer (EnT) as well.

Introduction

The influence of proton motion on electron transfer (ET) may be revealed by photoinducing fixed-distance ET across an intervening proton network[1–4] such as carboxylic acid dimers,[5,6] guanine-cytosine base pairs[7–9] and related interfaces[10,11] and amidinium-carboxylate salt bridges.[12–17] The coupling of the proton to the electron occurs by communication between the charge shift resulting from the motion of the proton and electron through the polarization of the surrounding environment.[18–20] Even in the absence of formal proton transfer, fluctuations of the proton position within the interface may exert significant influence over ET.[17,21,22] To this end, the possibility arises that the proton can also influence events that do not involve single ET. From the perspective of semiclassical models, the influence of the proton appears explicitly in the electronic coupling constant, $|V|$. Given that the electronic coupling elements for energy and electron transfer are related,[23] it is logical to consider that PCEnT would be manifested in the electronic coupling element for EnT.

We now explore this possibility by juxtaposing ferrocenyl (Fc) moieties to Ru(II) polypyridyl complexes, [Ru] = Ru(II)(bpy-COOH)$(L)_2^{2+}$ where L = btfmbpy (4,4′-*bis*(trifluoromethyl)-2,2′ bipyridine), $\mathbf{Ru^A}$, or bpy (2,2′-bipyridine), $\mathbf{Ru^B}$, *via* an amidinecarboxylic acid two-point hydrogen bond (–[H^+]–) to form a [Ru]–[H^+]–[Fc] supramolecular assembly. The excited states of these Ru(II) polypyridyl complexes can be

†Electronic supplementary information (ESI) available: Full experimental details and characterization of ferrocenyl amidinium compounds, and $\mathbf{Ru^B}$, spectroscopic and electrochemical data, Dexter energy transfer analysis and spectroscopic calculations. See DOI: 10.1039/c1sc00596k

Correspondence to: Daniel G. Nocera.

deactivated by ferrocene *via* either ET and EnT quenching.[24–28] The dominant quenching mechanism has generally been difficult to distinguish for previously studied systems in which the quenching process is bimolecular or the ferrocene moiety is tethered to the Ru(II) polypyridyl complex *via* a conformationally flexible alkane or alkene tether.[25–28] In these cases, the mechanism and quenching dynamics are obscured by diffusion or conformational changes. The [Ru]–[H^+]–[Fc] dyads described here obviate this problem by fixing the [Ru]–[Fc] distance with a strong hydrogen bonding amidinium-carboxylate interface. The distal separation between Ru and Fc can be tuned by varying the covalent linkage between the cyclopentadienyl (Cp) ring of the ferrocene moeity and amidine functionality. Methodologies are presented that permit the amidine to be fused directly to the Cp ring or appended to intervening phenylene or ethynyl spacers. Varying degrees of electronic communication between ferrocene and the pendant amidine are revealed by electrochemistry and UV-visible absorption spectroscopy. Transient spectroscopy and kinetic isotope studies establish proton-coupled energy transfer (PCEnT) as the dominant quenching process within [Ru]–[H^+]–[Fc] supramolecular assemblies.

Experimental

The suprmolcular dyads were prepared according to the pathways listed in Scheme 1. Preparation of the directly linked ferrocene-amidinium conjugate (**3**) was accomplished in two steps beginning with the lithiation of bromoferrocene (**1**) followed by reaction with phenyl cyanate (PhOCN).[29] Subsequent reaction with $Al(CH_3)(NH_2)Cl$ under harsh conditions delivers ferrocene-amidinium **3**. The phenyl linked ferrocene-amidinium conjugate (**5**) is delivered from 4-cyanophenylferrocene (**4**), which is furnished by Suzuki coupling of bromoferrocene (**1**) with 4-cyanophenylboronic acid. Reaction of **4** with Weinreb's amide transfer reagent[30] ($Al(CH_3)(NH_2)Cl$) ultimately generates amidinium derivative **5**. Preparation of the alkynyl linked ferrocenyl amidinium (**9**) is slightly more involved. Bromoferrocene (**1**) is converted to a trimethylsilyl protected alkynyl-ferrocene synthon (**6**) *via* Sonogashira coupling with trimethylsilylacetylene in the presence of a Cu(I) and Pd(II) catalyst. Deprotection under basic conditions delivers the terminal alkyne (**7**) and subsequent deprotonation and reaction with PhOCN generates the nitrile capped alkynyl-ferrocene derivative (**8**). Reaction of **8** with $Al(CH_3)(NH_2)Cl$ yields **9** in excellent yield. Detailed syntheses and characterization of all compounds are given in the Supporting Information.†

Time-resolved absorption (TA) and time-resolved emission (TE) measurements were performed by using the third harmonic (355 nm) of the 1064 nm fundamental of a pulsed Nd:YAG laser (Spectra-Physics Quanta-Ray PRO-Series) to pump an optical parametric oscillator (OPO) at a repetition rate of 10 Hz with pulse energies of ~340 mJ/pulse and pulse width of ~7 ns. This laser has been integrated into an experimental set-up for time-resolved emission and absorption studies as described elsewhere.[31] Variable temperature luminescence lifetime measurements were performed on a Hamamatsu C4334 Streak Scope streak camera. Variable-temperature emission spectra were recorded on an automated Photon Technology International (PTI) QM 4 fluorimeter equipped with a 150 W Xe arc lamp and a Hamamatsu R928 photomultiplier tube.

Absorption spectroscopy titrations with 4-dimethylaminopyridine (DMAP), time resolved emission experiments and temperature-dependent emission experiments were performed on samples contained in a high-vacuum cell comprised of a 1 cm pathlength clear fused-quartz

†Electronic supplementary information (ESI) available: Full experimental details and characterization of ferrocenyl amidinium compounds, and $\mathbf{Ru^B}$, spectroscopic and electrochemical data, Dexter energy transfer analysis and spectroscopic calculations. See DOI: 10.1039/c1sc00596k

cuvette (Starna cells) connected to a 10 cm^3 solvent reservoir *via* a graded seal. High-vacuum Teflon valves were used to seal the cell from the environment and the cuvette from the solvent reservoir. The sample manipulations employed for these experiments are described in detail in the Supporting Information.†

Electrochemical measurements were performed with a Bio-analytical Systems (BAS) Model CV – 50 W potentiostat/galvanostat. Differential pulse voltammetry (DPV) was performed using a glassy carbon working electrode, a Ag/AgCl reference electrode and a platinum wire auxiliary electrode. DPV experiments were preformed in CH_2Cl_2 with 0.1 M tetrabutylammonium perchlorate (NBu_4ClO_4) as the supporting electrolyte and in tetrahydrofuran (THF) with 0.1 M tetrabutylammonium hexafluorophosphate (NBu_4PF_6). Concentrations of ~1 mM were prepared for DPV experiments on **3**, **5**, **9**, **Ru^{A}**, and **Ru^{B}**. A scan rate of 100 mV s^{-1} and a sensitivity of 10 μA V^{-1} were used for data acquisition. Prior to each experiment, the solution was sparged with argon to eliminate dissolved O_2. All potentials are reported *versus* the Ag/AgCl reference electrode.

Results

The syntheses of the ferrocenyl amidinium complexes **3**, **5** and **9** proceed by the pathways of Scheme 1. A highly efficient and modular route to these ferrocene amidinium complexes is afforded by using bromoferrocene (**1**)[32] as a starting material for all three derivatives. The introduction of the amidinium unit on the Cp rings of ferrocene follows a strategy that is similar to that used for the preparation of porphyrin amidinium derivatives,[33–36] namely, the conversion of ferrocene-nitrile derivatives (**2**, **4** and **8**) to the corresponding amidiniums using Weinreb's amide transfer reagent.[30] Complete details of compound synthesis and characterization are provided in the Supporting Information.†

Electronic coupling between the [Fc] redox site and the protonic interface is evident from the effect of protonation state on the electronic absorption spectra of each of the ferrocenyl amidiniums. As we have observed for amidinium porphyrins,[36,37] the absorption spectra of **3**, **5** and **9** each display a hypsochromic shift upon amdinium deprotonation (Fig. S1†). The extent of that shift is a measure of the electronic communication of the amidine with the metal complex to which it is appended. Complex **9** exhibits the largest hypsochromic shift. The cylindrical electronic symmetry of the ethynyl spacer ensures that the amidinium remains strongly electronically coupled regardless of the rotation angle assumed by the amidinium.[37] The pK_a of the amidinium is determined by Benesi–Hildebrand analysis of the shifting absorption spectrum as a function of deprotonation.[38] Fig. S2† plots the spectral shifts of the absorption band of **3** and **9** upon their titration with DMAP. The ratio of the *y*-intercept to the slope of linear fit of a plot of $1/\Delta A_{MLCT}$ *vs.* 1/[DMAP] furnishes the deprotonation constant, K_a'; values of K_a'(**3**) = 6.44 × 10^2 M and K_a'(**9**) = 1.65 × 10^2 M are obtained. Determination of the ferrocene-amidinium pK_a value is accomplished using the relation,

$$\mathrm{p}K_\mathrm{a}\left(\mathrm{am}^+\right) = \mathrm{p}K_\mathrm{a}\left(\mathrm{DMAP}\right) - \log\left(K_\mathrm{a}{}'\right) \quad (1)$$

The pK_a' of DMAP in CH_3CN is 12.33,[39] yielding pK_a values of pK_a(**3**) = 9.52 ± 0.10 and pK_a(**9**) = 10.11 ± 0.10. The small spectral shifts displayed by **5** upon titration with base together with spectral congestion precluded an accurate determination of the pK_a of this derivative. Notwithstanding, we expect the pK_a of **3** and **5** to be similar based on the congruence of their spectral shifts (Δ*E*shift = 193 cm^{-1} and 217 cm^{-1}). Considering the pK_a values of carboxylic acids (pK_a benzoic acid ~20 and the pK_a of acetic acid ~20–22) in

CH_3CN,[39] the –[H^+]– interface should be non-ionized (*i.e*. amidine–carboxylic acid), as has been established previously.[40]

The redox thermodynamics for **Ru^{A}**, **Ru^{B}**, **3**, **5**, and **9** in CH_2Cl_2 and THF were characterized by DPV. The DPV traces for each compound are shown in Fig. S3.† The reduction and oxidation potentials of the compounds in CH_2Cl_2 are: E_p(**3**) = 0.84 V; E_p(**5**) = 0.66 V; E_p(**9**) = 0.51 V; E_p(**Ru^{A}**) = −0.74 V; E_p(**Ru^{B}**) = −1.33 V. The perturbation of the redox potential upon salt bridge formation was assessed by measuring the DPVs of **Ru^{A}** and **Ru^{B}** upon the incremental addition of phenylamidine (**Ph-am**), which efficiently binds to the carboxylic acid of the Ru complex, but is redox inactive (Fig. S4†). Only a 24 and 30 mV increase is observed in E_p for **Ru^{A}** (up to 30 eq of **Ph-am**) and **Ru^{B}** (up to 50 eq), respectively. Thus the redox properties of the Ru complexes are expected to be perturbed insignificantly upon formation of the amidine–carboxylic acid interface within the [Ru]–[H^+]–[Fc] dyads.

Time-resolved emission experiments were undertaken on each of the six possible D–A combinations. Emission quenching is observed for all dyads studied; quenched (τ) and unquenched (τ_q) time constants for each system are compiled in Table 1. The lifetime of **Ru^{A}** or **Ru^{B}** excited states (τ_0) in the absence of a ferrocenyl amidinium conforms to a monoexponential decay. The unquenched lifetimes of **Ru^{A}** and **Ru^{B}** are 0.84 μs and 1.25 μs, respectively. By contrast, for solutions of **Ru^{A}** or **Ru^{B}** in the presence of either **3**, **5** or **9**, a biexponential decay is observed, which corresponds to the excited state deactivation of unassociated **Ru^{A}** and **Ru^{B}** and their decay within the associated complexes **Ru^{A}:Fc** or **Ru^{B}:Fc**. The quenching rate constant is determined from the relation $k_q = \tau^{-1} - \tau_0^{-1}$. The quenching data exhibits a kinetic isotope effect (KIE) for [Ru]–[D^+]–[Fc] supra-molecular assemblies. These data are also shown in Table 1 for the six dyads.

Based on the excited state energy of the [Ru] complexes and the redox potentials of the six D–A dyads, a favorable driving force for ET (0 eV > $-\Delta G_{ET}$ > 0.8 eV) is established between **Ru^{A}** and **Ru^{B}**, and **3**, **5** and **9** (Table S1†). Transient absorption spectroscopy was undertaken to search for evidence of a charge separated (CS) state, which would be indicative of a ET quenching pathway. However, no spectral signatures attributed to a CS species were observed. The absence of a CS signature does not necessarily exclude ET as the dominant quenching mechanism if the back ET reaction is significantly accelerated with regard to the forward ET reaction. For such a case, the charge transfer intermediate will not accumulate to detectable levels. Other potential quenching mechanisms include EnT *via* Dexter (DEnT) or Förster resonance energy transfer (FRET). For the latter, as calculated in the Supporting Information,† the overlap integral for FRET is negligible and results in predicted FRET rates that are 10–200 times slower than the rates observed.

With the FRET mechanism discarded, the two possible primary mechanisms are ET and DEnT. Both processes can be analyzed under the semi-classical formalism to describe rates of nonradiative processes:

$$k_q = \frac{4\pi^2}{h} \bullet |V^2| \bullet \frac{1}{\sqrt{4\pi\lambda k_B T}} \bullet \exp\left(-\frac{(\Delta G_0 + \lambda)^2}{4\lambda k_B T}\right) \quad (2)$$

where ΔG_o is the free energy change associated with the reaction, λ is the solvent reorganization energy of the process, and $|V|$ is the electronic coupling constant between the donor and acceptor. Of particular importance in distinguishing between ET and DEnT is the solvent reorganization term. Since only small charge redistributions occur within the MLCT excited state of the Ru(II) polypyridyl complexes, very little charge accrues during DEnT and λ should be significantly less for EnT than ET. For Ru(II) polypyridyl complexes, inner

sphere reorganization λ_i is minimal so that most of λ is determined by the outer sphere DEnT reorganization energy, *i.e.*, $\lambda \sim \lambda_o$. Typical λ_o values are ~1–2 eV for ET processes,[41] whereas they are ~0.1–0.2 eV for processes.[42–45]

The reorganization energy may be determined from the temperature dependence of the emission bandwidth, $\Delta\bar{\nu}_{0,1/2}$. For the Ru(II) polypyridyl comlexes, **Ru^{A}** and **Ru^{B}**, the emission spectra bandwidth reflects the reorganization energy associated with conversion of the MLCT excited state to the ground state. The temperature-dependence of the square of fitted emission bandwidth is related to the outer sphere reorganization energy, λ_o, is given by,[46–48]

$$\left(\Delta\bar{\nu}_{0,1/2}\right)^2 = \left(\Delta\bar{\nu}^{0}_{0,1/2}\right)^2 + 16\,(ln2)\,\lambda_o \mathrm{k}_B T \quad (3)$$

Fig. 1 plots $\left(\Delta\bar{\nu}_{0,1/2}\right)^2$ *versus* temperature; the slope of the line of this fit yields λ_o. Analysis of these data with eqn (3) yields λ_o (**Ru^{A}:3**) = 0.102 eV and λ_o(**Ru^{B}:3**) = 0.050 eV. These values are very similar to the outer-sphere reorganization energies of the control systems in which there is no energy accepting [Fc] moiety, λ_o(**RuA:Ph-am**) = 0.12 eV and λ_o(**RuB:Ph-am**) = 0.11 eV. The λ_o values are significantly less than the λ_o = 0.85 eV calculated from Marcus theory for the ET reaction of these dyads.[49] These results taken together with the inability to observe charge transfer products in time-resolved absorption spectra support the assignment of DEnT as the quenching mechanism in **Ru^{A}:3** and **Ru^{B}:3**. A similar DEnT quenching pathway is expected when **5** or **9** serves as the acceptor.

The proton-coupling of energy transfer *via* the electronic coupling matrix element is directly revealed by the KIEs listed in Table 1. Whereas [Ru^{A}]–[H^{+}]–[Fc] exhibits a normal KIE, an inverse KIE is observed for [Ru^{B}]–[H^{+}]–[Fc]. Theoretical treatments of PCET have shown that small fluctuations within the interface can dynamically modulate electronic coupling, and consequently the rate of transfer becomes sensitive to the nature of proton vibrational modes within the bridge.[21] Proton interfaces that are not as tightly bound require the proton or deuteron positions to fluctuate by larger amounts in order to induce ET. Because the tails of the proton or deuteron wavefunctions dictate the efficacy of proton tunneling. In such cases, the overlap of the more diffuse proton wavefunction is greater than the overlap of the more localized deuteron wavefunction and a normal KIE is expected (Fig. 2). However, in a more tightly coupled interface, the overlap of the deuteron wavefunction at its equilibrium position with the critical displacement may be greater than the overlap between the proton wavefunction at its equilibrium point. Provided that only small fluctuations of the hydrogen bond are required to attain the equilibrium configuration, an inverse KIE is predicted. Inasmuch as the ET and EnT process are related *via* the electronic coupling matrix element,[23] parallels may be drawn between the KIEs of proton-coupled ET and EnT events.

The disparate behavior of the two [Ru] complexes likely stems from the differing nature of the MLCT excited states of the two systems. Soler and McCusker have shown[50] that Ru(II) polypyridyl complexes covalently bound to dinuclear manganese complexes possess electronic coupling constant that are two orders of magnitude greater when the excited state is localized on the bridging bpy ligand as opposed to the ancillary ligand. Along these lines, Raman studies of functionalized Ru(II) bpy complexes reveal that the electron localizes on the bpy ligands bearing the most electron withdrawing functionality. Hence the MLCT excited state of **Ru^{B}** is centered on the bridging bpy ligand connected to the –[H^{+}]– interface, whereas excitation of the MLCT state of **Ru^{A}** produces an excited state localized on the fluorinated bpy ligands, remote from the –[H^{+}]– interface.

Conclusions

The supramolecular assembly of ferrocenyl-amidinium compounds with two Ru(II) polypyridyl complexes allows for the study of hydrogen-bond mediated quenching through well-defined two-point interfaces. Measurement of the pK_a of the amidinium affixed to the Cp ring of ferrocene establishes that the two-point hydrogen bonded interface is not that of the salt bridge but is formed from the association of amidine with carboxylic acid. The excited state of Ru(II)(bpy-COOH)$(L)_2^{2+}$ where L = btfmbpy (4,4′-*bis*(trifluoro-methyl)-2,2′-bpy) or bpy (2,2′-bipyr-idine) is efficiently quenched by the juxtaposed ferrocene, which is electronically coupled to the Ru(II) polypyridyl excited state *via* the amidine-carboxylic acid salt bridge. Transient and temperature-dependent spectroscopic measurements reveal that the small reorganization energy attendant to the quenching process is consistent with energy transfer rather than electron transfer. Moreover, an observed kinetic isotope effect on the quenching process indicates that the proton dependence on EnT arises *via* the electronic coupling term between the [Ru] EnT donor and the [Fc] EnT acceptor. To this end, the mechanism of PCEnT is similar to that of PCET; *i.e*., the electronic coupling matrix element modulates the transfer of energy in PCEnT, as it also does for the transfer of an electron in a PCET reaction. These results on an inorganic-based EnT system add to the emerging trend of organic-based EnT systems[51–54] that energy transfer can be mediated by proton-transfer interfaces.

Supplementary Material

Refer to Web version on PubMed Central for supplementary material.

Acknowledgments

This work was performed under the auspices of the National Institutes of Health (GM47274). J. R. thanks the Fannie and John Hertz Foundation for financial support. We thank Prof. Masaoki Furue for providing $Ru(btfmbpy)_2Cl_2$, which was used as a precursor for the preparation of **Ru^A**.

Notes and references

1. Cukier RI, Nocera DG. Annu. Rev. Phys. Chem. 1998; 49:337–369. [PubMed: 9933908]
2. Chang CJ, Chang MCY, Damrauer NH, Nocera DG. Biochim. Biophys. Acta, Bioenerg. 2004; 1655:13–28.
3. Reece SY, Hodgkiss JM, Stubbe J, Nocera DG. Philos. Trans. R. Soc. London, Ser. B. 2006; 361:1351–1364. [PubMed: 16873123]
4. Reece SY, Nocera DG. Annu. Rev. Biochem. 2009; 78:673–699. [PubMed: 19344235]
5. Turró C, Chang CK, Leroi GE, Cukier RI, Nocera DG. J. Am. Chem. Soc. 1992; 114:4013–4015.
6. de Rege PJF, Williams SA, Therien MJ. Science. 1995; 269:1409–1413. [PubMed: 7660123]
7. Sessler, JL.; Wang, B.; Springs, SL.; Brown, CT. Comprehensive Supramolecular Chemistry. Murakami, Y., editor. Vol. vol. 4. Pergamon Press; Oxford: 1996. p. 311-336.
8. Ward MD. Chem. Soc. Rev. 1997; 26:365–375.
9. Shafirovich VY, Courtney SH, Ya N, Geacintov NE. J. Am. Chem. Soc. 1995; 117:4920–4929.
10. Ghaddar TH, Castner EW, Isied SS. J. Am. Chem. Soc. 2000; 122:1233–1234.
11. Chang, CJ.; Brown, JDK.; Chang, MCY.; Baker, EA.; Nocera, DG. Electron Transfer in Chemistry. Balzani, V., editor. Vol. Vol. 3.2.4. Wiley-VCH; Weinheim, Germany: 2001. p. 409-461.
12. Damrauer NH, Hodgkiss JM, Rosenthal J, Nocera DG. J. Phys. Chem. B. 2004; 108:6315–6321. [PubMed: 18950117]
13. Roberts JA, Kirby JP, Nocera DG. J. Am. Chem. Soc. 1995; 117:8051–8052.
14. Kirby JP, Roberts JA, Nocera DG. J. Am. Chem. Soc. 1997; 119:9230–9236.

15. Roberts JA, Kirby JP, Wall ST, Nocera DG. Inorg. Chim. Acta. 1997; 263:395–405.
16. Kirby JP, Roberts JA, Nocera DG. J. Am. Chem. Soc. 1997; 119:9230–9236.
17. Hodgkiss JM, Damrauer NH, Pressé S, Rosenthal J, Nocera DG. J. Phys. Chem. B. 2006; 110:18853–18858. [PubMed: 16986876]
18. Hammes-Schiffer S, Stuchebrukhov AA. Chem. Rev. 2010; 110:6939–6960. [PubMed: 21049940]
19. Cukier RI. Biochim. Biophys. Acta, Bioenerg. 2004; 1655:37–44.
20. Hammes-Schiffer S. Acc. Chem. Res. 2001; 34:273–281. [PubMed: 11308301]
21. Pressé S, Silbey R. J. Chem. Phys. 2006; 124:164504–164510. [PubMed: 16674143]
22. Hammes-Schiffer S. J. Phys. Chem. Lett. 2011; 2:1410–1416.
23. Closs GL, Johnson MD, Miller JR, Piotrowiak P. J. Am. Chem. Soc. 1989; 111:3751–3753.
24. Lee EJ, Wrighton MA. J. Am. Chem. Soc. 1991; 113:8562–8564.
25. Fery-Forgues S, Delavaux-Nicot B. J. Photochem. Photobiol., A. 2000; 132:137–159.
26. Siemling U, Vor der Bueggen J, Vorfeld U, Neumann B, Stammler A, Stammler H-G, Brockhinke A, Plessow R, Zanello P, Laschi F, de Biani FF, Fontani M, Steenken S, Stapper M, Gurzadyan G. Chem.–Eur. J. 2003; 9:2819–2833. [PubMed: 12866548]
27. Delgadillo A, Leiva AM, Loeb B. Polyhedron. 2005; 24:1749–1754.
28. Heinze K, Hempel K, Beckmann M. Eur. J. Inorg. Chem. 2006; 10:2040–2050.
29. Moss RA, Chu G, Sauers RR. J. Am. Chem. Soc. 2005; 127:2408–2409. [PubMed: 15724992]
30. Levin JI, Turos E, Weinreb SM. Synth. Commun. 1982; 12:989–993.
31. Loh Z-H, Miller SE, Chang CJ, Carpentar SD, Nocera DG. J. Phys. Chem. A. 2002; 106:11700–11708.
32. Lai LL, Dong T-Y. Synthesis. 1995; 10:1231–1233.
33. Deng Y, Chang CK, Nocera DG. Angew. Chem., Int. Ed. 2000; 39:1066–1068.
34. Kirby JP, van Dantzig NA, Chang CK, Nocera DG. Tetrahedron Lett. 1995; 36:3477–3480.
35. Yeh C-Y, Miller SE, Carpenter SD, Nocera DG. Inorg. Chem. 2001; 40:3643–3646. [PubMed: 11421722]
36. Rosenthal J, Hodgkiss JM, Young ER, Nocera DG. J. Am. Chem. Soc. 2006; 128:10474–10483. [PubMed: 16895413]
37. Rosenthal J, Young ER, Nocera DG. Inorg. Chem. 2007; 46:8668–8675. [PubMed: 17854170]
38. Connors, KA. Binding Constants: A Measurement of Molecular Complex Stability. Wiley; New York: 1987.
39. Izutsu, K. Acid–base Dissociation Constants in Dipolar Aprotic Solvents. Blackwell Scientific; Cambridge, USA: 1990.
40. Young ER, Rosenthal J, Nocera DG. Chem. Commun. 2008:2322–2324.
41. Gray HB, Malmstrom BG, Williams RJP. JBIC, J. Biol. Inorg. Chem. 2000; 5:551–559.
42. Barigelletti R, Flamigni L, Guardigli M, Juris A, Beley M, Chodorowski-Kimmes S, Collin J-P, Savauge J-P. Inorg. Chem. 1996; 35:136–142. [PubMed: 11666175]
43. Hamada T, Tanaka S, Koga H, Sakai Y, Sakaki S. J. Chem. Soc. Dalton Trans. 2003:692–698.
44. Liard DJ, Kleverlaan CJ, Vlcek A. Inorg. Chem. 2003; 42:7995–8002. [PubMed: 14632518]
45. Indelli MT, Bignozzi CA, Harriman A, Schoonover JR, Scandola F. J. Am. Chem. Soc. 1994; 116:3768–3779.
46. Kober EM, Casper JV, Lumpkin RS, Meyer TJ. J. Phys. Chem. 1986; 90:3722–3734.
47. Opperman KA, Mecklenburg SL, Meyer TJ. Inorg. Chem. 1994; 33:5295–5301.
48. Claude JP, Meyer TJ. J. Phys. Chem. 1995; 99:51–54.
49. The outer-sphere reorganization energy can be calculated using the Marcus dielectric continuum model for the systems in a solvent of given dielectric constant using the relation: $\lambda_s = 14.4\left(\frac{1}{2r_D} + \frac{1}{2r_A} - \frac{1}{d_{DA}}\right) \times \left(\frac{1}{\varepsilon_\infty} - \frac{1}{\varepsilon_s}\right)$ where r_D and r_A are the ionic radii of the donor and acceptor, respectively, d_{DA} is the D–A separation, ε_∞ is equal to the refractive index of the solvent squared, and ε_s is dielectric constant of the solvent. The refractive index and dielectric constant for CH_2Cl_2 are 1.4212 and 8.93, respectively. The ionic radii of 3 is 3.2 Å; 5 is 7.3 Å; 9

is 5.5 Å; **RuA** is 6 Å; and **RuB** is 6 Å. D–A separation for **RuA** and **RuB** with **3**, **5**, and **9** is 12.6 Å;, 16.8 Å, and 14.8, respectively.

50. Soler M, McCusker JK. J. Am. Chem. Soc. 2008; 130:4708–4724. [PubMed: 18341336]
51. Vinita M, Hirdyesh M. J. Chem. Phys. 2008; 128:244701–244708. [PubMed: 18601359]
52. Moitrayee M, Shreetama K, Tapas C. J. Phys. Chem. A. 2011; 115:1830–1836. [PubMed: 21329362]
53. Sarkar D, Mahata A, Das P, Girigoswami A, Chattopadhyay N. Chem. Phys. Lett. 2009; 474:88–92.
54. Ghosh D, Bose D, Sarkar D, Chattopadhyay N. J. Phys. Chem. A. 2009; 113:10460–10465. [PubMed: 19728699]

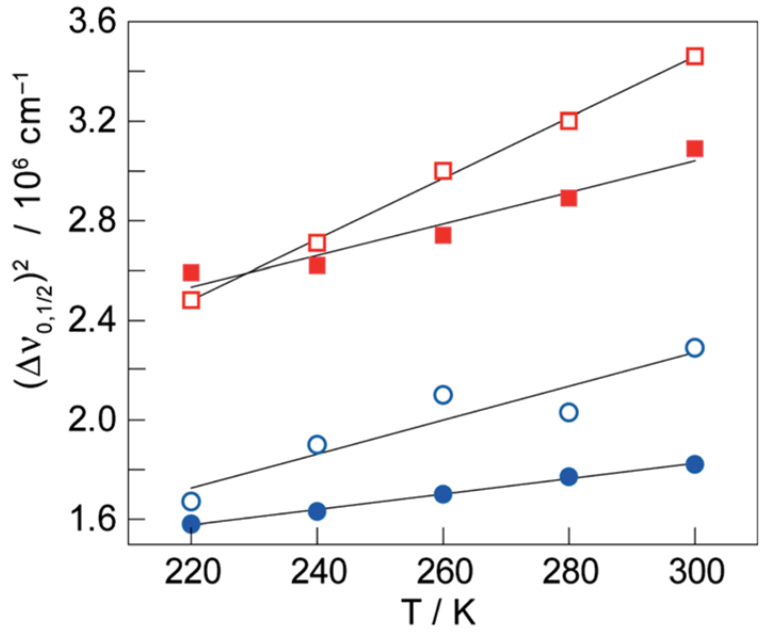

Fig. 1.

Temperature dependence of full-width-at-half- maximum $(\Delta\nu_{0,1/2})^2$ of emission from **Ru^{A}**:Ph-am (□), **Ru^{A}:3 (.)**, **Ru^{B}**:Ph-am (◯), and **Ru^{B}:**3 (●).

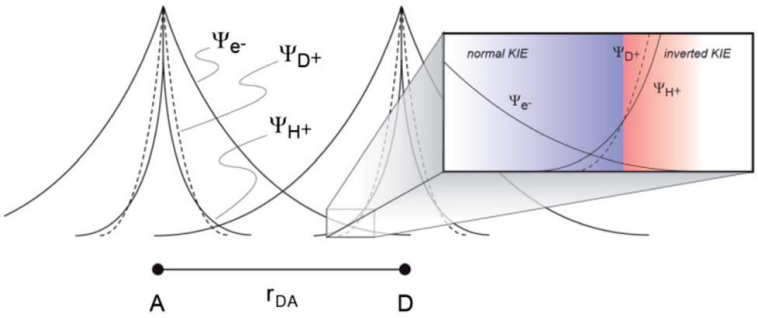

Fig. 2.

Proton fluctuations within the amidinium-carboxylic acid interface may dynamically modulate electronic coupling for PCEnT, and consequently the rate of transfer becomes sensitive to the nature of proton vibrational modes within the bridge. Under typical conditions, wavefunction overlap of the deuterated bridge is smaller than that of the proton and a normal KIE is observed and is shown schematically in the left (blue shaded region). However, thermal population of vibrational excited states may be a cause of the reverse isotope effect in this system, where the low frequency mode of interest is a localized 3-atom N–H–O vibration in the hydrogen bond (red shaded region).

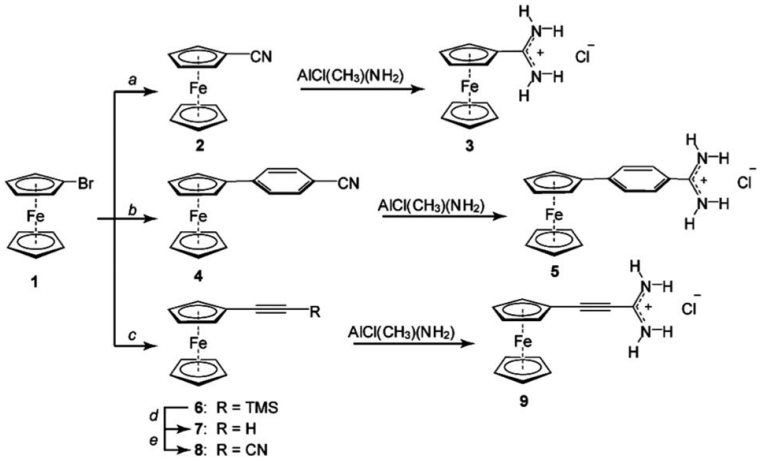

(a) 1. CH_3Li; 2. PhOCN; (b) $(dppf)Pd(Cl)_2$, Na_2CO_3, 4-cyanophenylboronic acid, THF, H_2O; (c) (Trimethylsilyl)acetylene, CuI, $PdCl_2(PPh_3)_2$, NEt_3, DMF; (d) K_2CO_3, THF, CH_3OH; (e) 1. CH_3Li, THF; 2. PhOCN.

Scheme 1.
Synthetic schemes for the preparation of amidinium ferrocene compounds

Table 1

Quenching rate constants of [Ru]-Fc dyads[a]

	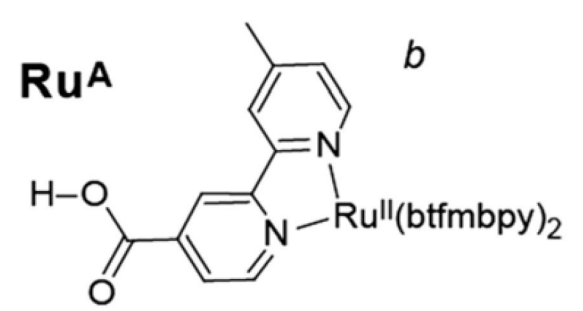			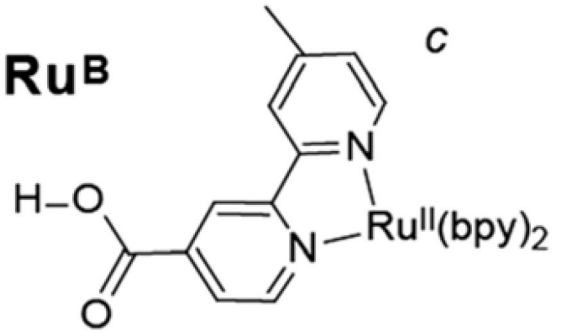		
[RU]–[H$^+$]–Fc	**t/μs**	**$k_q/10^6$ s^{-1}**	**KIE**	**t/μs**	**$k_q/10^6$ s^{-1}**	**KIE**
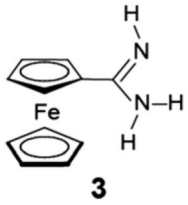 **3**	0.176	4.5(2)	1.62	0.386	1.79(3)	0.55
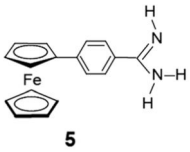 **5**	0.223	3.3(3)	3.14	0.166	5.22(5)	0.90
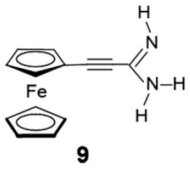 **9**	0.280	2.38(9)	1.25	0.235	3.45(7)	0.84

[a] All data recorded in DCM at 298 K.

[b] Unquenched lifetime of **Ru^A** is 0.84 μs.

[c] Unquenched lifetime of **Ru^B** is 1.25 μs.